Direct measurement of coherent subterahertz acoustic phonons mean free path in GaAs

R. Legrand, A. Huynh, B. Jusserand, and B. Perrin*
Sorbonne Universités, UPMC Univ. Paris 06, CNRS-UMR 7588, Institut des Nanosciences de Paris, F-75005 Paris, France

A. Lemaître
CNRS, UPR 20, Laboratoire de Photonique et de Nanostructures, Route de Nozay, F-91460 Marcoussis, France
(Received 28 September 2015; revised manuscript received 19 February 2016; published 19 May 2016)

The phonon mean free path is generally inferred from the measurement of thermal conductivity and we are still lacking precise information on this quantity. Recent advances in the field of high-frequency phonons transduction using semiconductor superlattices give the opportunity to fill this gap. We present experimental results on the attenuation of longitudinal acoustic phonons in GaAs in the frequency and temperature ranges 0.2–1 THz and 10–80 K respectively. Surprisingly, we observe a plateau in the frequency dependence of the attenuation above 0.7 THz, that we ascribe to a breakdown of Herring processes.

DOI: 10.1103/PhysRevB.93.184304

I. INTRODUCTION

A large renewed interest appeared recently in theoretical and experimental studies of phonons mean free paths (MFP) in semiconductors. Thermal transport in optoelectronic and microelectronic devices and engineering of new thermoelectric systems are strongly dependent on this parameter, which is still not very well known. A series of recent experiments using thermal conductivity spectroscopy technique [1–6] showed that phonons contributing to thermal conductivity have a large distribution of MFP. It can be suspected that low-frequency phonons may have MFP in the micrometric range at room temperature and thus could play a large role in heat transport in nanosystems [7–9]. In addition, first-principles calculations [10–12] proved that the simplistic kinetic theory based on an averaged phonon MFP value can be very misleading. In this context accurate and direct MFP measurements for well-defined individual subterahertz phonon modes would be useful. In this paper, we present experimental measurements of the attenuation of coherent longitudinal acoustic waves propagating along [100] with frequencies going from 0.2–1 THz in the temperature range 10–80 K. Direct phonon MFP measurements in the subterahertz range cannot be done with a good accuracy by inelastic neutron and x-ray scattering and is out of reach for standard light scattering methods. Picosecond ultrasonics methods combined with metallic films as transducers have been used up to 0.1 THz for MFP determinations in bulk samples [13–16] and a few hundreds of GHz in strongly absorbing amorphous thin films [17,18]. Recently, semiconducting superlattices (SL) proved to be very efficient emitters and detectors of subterahertz coherent acoustic waves [19–26] and have also been used for phonon MFP measurements [27–29]. Excited by a femtosecond laser pulse with an energy above the electronic band gap, a SL can emit a discrete set of frequencies determined by its period superimposed on a low-frequency spectrum extending up to a few tens of GHz. The discrete frequencies correspond to the lower edges of phonon energy gaps at the center of the Brillouin zone $\mathbf{q}_{ac} = \mathbf{0}$ where $\mathbf{q}_{ac}$ is the acoustic wave vector. These SLs may also resonantly detect any mode satisfying the selection rule $\mathbf{q}_{ac} = \mathbf{k}_i + \mathbf{k}_d$ where $\mathbf{k}_i$ and $\mathbf{k}_d$ are the incident and scattered electromagnetic wave vectors. Furthermore, the detection is strongly enhanced if the probe laser wavelength is tuned closed to a SL electronic interband transition [30]. In spite of this wave vector mismatch between emission and detection, it is possible to emit and detect phonons using a single SL configuration but this is not the optimal way to perform experiments. A series of measurements was conducted in different configurations in order to access the attenuation of longitudinal phonons at several frequencies up to 1 THz as a function of temperature. A striking feature was obtained with the observation of a plateau in the frequency dependence. We analyze the different absorption processes that exist in these temperature and frequency domains, with a special attention on Herring processes [31]. The paper is organized as follows. In Sec. II, experimental methods and studied samples are introduced. Section III presents experimental results and a discussion on the data.

II. SAMPLES AND EXPERIMENTAL DETAILS

The interaction of a femtosecond laser pulse with a SL results in the emission of a coherent acoustic pulse, which is launched into the underlying substrate. The pulse contains a few narrow frequency components mostly defined by the period of the SL. After propagation, it can be detected either by another SL grown on the opposite side of the substrate or by the same SL after a round trip through the wafer. In both cases, the acoustic strain induces a change of reflectivity, measured by a probe laser light. We use a femtosecond Ti:Sapphire mode-locked laser providing 80 fs pulses (∼200 fs pulses incoming on the sample), operating at a wavelength that has been tuned between 680–820 nm, depending on the SL period, with a repetition rate of 80 MHz. The pump is modulated at 1 MHz to allow synchronous detection through a lock-in amplifier. The control of the sample temperature is carried out using a He cryostat in exchange gas. Light beams are focused to a diameter of 60 μm, and typical energies per pulse amount to 0.5 nJ for the pump and 0.2 nJ for the probe.

We used four different configurations: (i) reflection experiments on a single SL (S400), which acts both as a phonon

*Corresponding author: bernard.perrin@insp.jussieu.fr

TABLE I. Characteristics of the samples. LP is a superlattice with a large period. DS400 to DS1000 contain two SLs on each side of the substrate, one of which presents a thickness gradient of all layers. The characteristics done here correspond to the uniform SL. RT denotes round trip, Trans denotes transmission, and (i) to (iv) refer to the description of experimental configurations.

Sample	$q_{ac} = 0$ mode frequency (THz)	Studied frequency (THz)	Thicknesses GaAs/AlAs (nm)	Number of periods	Substrate thickness (μm)	Experimental configuration	Propagation distance (μm)
LP	0.202	0.202–0.243	17/113[a]	20.5	375	RT (iii)	750
S300	0.292	0.292	12.2/4.8	26.5	364	RT (ii)	738
S400	0.394	0.394	8.6/3.9	80	346	RT (i)	692
DS400a	0.394	0.394	8.9/3.5	100	360	Trans (iv)	360
DS400b	0.394	0.356–0.394	8.9/3.5	100	983	Trans (iv)	983
DS700	0.715	0.715	4.71/1.83	175	368	Trans (iv)	368
DS800	0.787	0.787–0.819	4.35/1.72	200	361	Trans (iv)	361
DS1000	1.008	1.008	3.48/1.38	250	368	Trans (iv)	368

[a]The reflectors layers are GaAs/$Ga_{0.2}Al_{0.8}As$.

emitter and detector; (ii) reflection experiments on a single SL (S300) embedded in an optical cavity, which strongly modifies the selection rule [32–34]; (iii) reflection experiments on a SL (LP) with a large period Λ such as $\mathbf{k}_i + \mathbf{k}_d = \mathbf{0}$ (mod $2\pi/\Lambda$); and, lastly, (iv) transmission experiments with slightly different SLs deposited on the opposite sides of a wafer in order to satisfy simultaneously the emission and detection selection rules (DS400a up to DS1000).

AlAs/GaAs superlattices were grown by molecular beam epitaxy on (001) oriented two-sided polished GaAs substrates. In all samples (except LP) the thicknesses d_1 and d_2 were chosen to have $\frac{3}{4}\lambda$ GaAs and $\frac{1}{4}\lambda$ AlAs layers, where λ is the wavelength of the emitted longitudinal acoustic wave; this condition gives the largest width for the first zone-center gap. Sample S300 is made of a single SL (working at 0.292 THz), which is embedded in an optical cavity, whose reflectors are formed by 56/65 nm GaAs/$Al_{0.2}Ga_{0.8}As$ distributed Bragg reflectors (three pairs for the top mirror and ten pairs for the bottom mirror). Samples labeled S400a up to S1000 are formed by two nearly identical SLs grown on both sides of the GaAs substrate. The growth is performed in two steps, one SL after another. The first SL has a uniform period but during the second SL growth, the suppression of the substrate wafer rotation yields to a gradient in the thickness of all layers, which is estimated to be of the order of 20% for the whole 2-in wafer. The presence of the thickness gradient on one SL allows to tune the detection spectral response to optimize the detection of the phonon generated by the uniform SL, after propagation through the substrate [24]. The role of emitter/detector of the SLs could be inverted in sample DS800, that explains that two values of frequencies could be reached (0.787 and 0.819 THz). At last, the sample labeled LP is a SL with a large period of 130 nm (labeled LP) made of 113/17 nm period $Ga_{0.2}Al_{0.8}As$/GaAs building block. The characteristics of the samples and the nine frequencies at which our experiments have been performed are summarized in Table I.

Below 0.4 THz the amplitude of the acoustic waves having made a round trip in the sample has been measured as a function of temperature. Above 0.4 THz, the reflection coefficient of acoustic waves on the sample backside can be strongly affected by its quality and cleanness. To avoid reflection losses, the acoustic attenuation for the highest frequencies has been obtained recording the high-frequency component just transmitted through the sample and detected with a SL deposited on the wafer backside [24].

III. RESULTS AND DISCUSSION

In our experimental configuration, we can only measure the relative change with temperature of the sound absorption coefficient $\Delta\alpha$, defined by

$$\Delta\alpha(T) = \frac{1}{d} \ln\left(\frac{A(T_0)}{A(T)}\right), \tag{1}$$

where d is is the propagation distance, $A(T_0)$ the amplitude of the discrete Fourier component at frequency ν_{ac} of the time-resolved detected signal, at the lowest temperature we could achieve (about 10 K), and $A(T)$ the same amplitude at temperature T. Experimental results are shown in Fig. 1. For frequencies up to 0.4 THz, the attenuation increases with temperature and frequency as can be expected [35]. Surprisingly, above 0.7 THz, a plateau appears in the frequency dependence. In order to get rid of possible artifacts, complementary experiments were undertaken. Indeed, this feature could also be attributed to (i) nonlinear interactions between

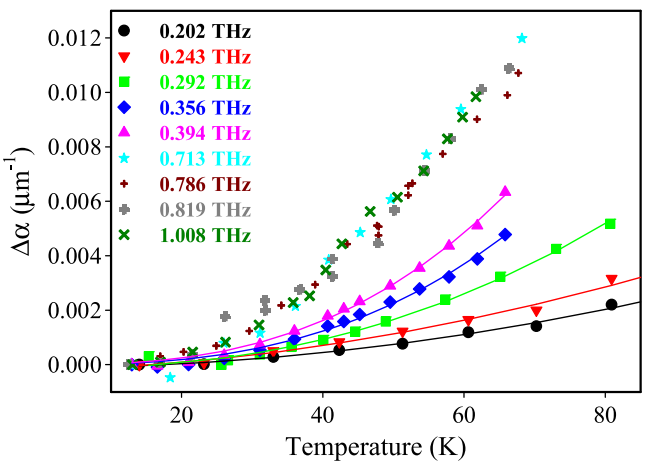

FIG. 1. Deviational sound absorption curves $\Delta\alpha(T)$. The colored full lines are a guide for the eye.

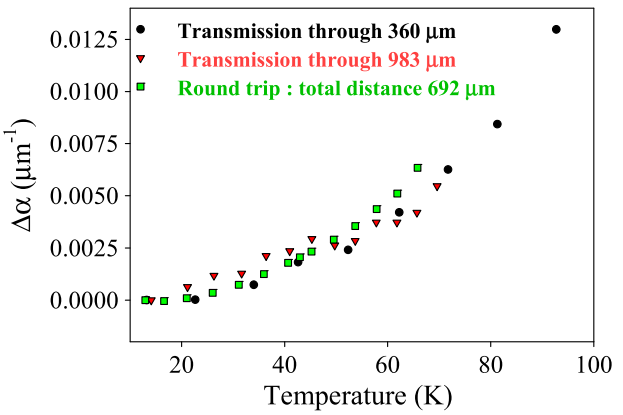

FIG. 2. Deviational sound absorption curves $\Delta\alpha$ obtained at 0.4 THz for different propagation distances.

the discrete high frequencies of the generated spectrum and its lower continuous part, however, pump laser power has been varied by a factor 30 and no difference was observed; or (ii) to the proximity of the probe wavelength to a SL electronic transition where photoelastic coefficients are very high [30]. We indeed can suspect that the SL properties slightly change with temperature. This would affect the measured acoustic wave amplitude signal. To check this point several tests were carried out. First, we renormalized the amplitudes of high-frequency components of the spectrum by the amplitude of low frequency (amplitude of echoes envelopes observed with an interferometric detection or Brillouin component at 40 GHz) for which $\Delta\alpha$ is negligible on our temperature range. In another set of measurements, the signal was optimized for each temperature by tuning the wavelength. In both cases, no significant difference was observed on the values of $\Delta\alpha$. Last, a more crucial test was performed by comparing experiments done at 0.4 THz for three different propagation distances. Any dependence of the emitters and detectors efficiencies on temperature would have had the most important effect for the shorter distances. As it can be seen in Fig. 2, the three sets of data obtained for the three different distances give the same results for $\Delta\alpha$ within an error bar of roughly 15%.

Having discarded most probable experimental sources of error, we have investigated the possible mechanisms responsible for this unexpected behavior. Two attenuation mechanisms have to be considered in the very low temperature limit. The spontaneous anharmonic decay of phonons gives a contribution $\alpha_{sd}(\mu\mathrm{m}^{-1}) = 1.31 \times 10^{-4}\nu^5$ as estimated by Berke [36], where the acoustic frequency ν is expressed in THz. The second mechanism (when the dopant concentration is low) is the isotopic scattering which gives a contribution [37] $\alpha_{\mathrm{iso}}(\mu\mathrm{m}^{-1}) = 7.5 \times 10^{-4}\nu^4$. Both contributions are rapidly overtaken by scattering processes and fission processes when temperature increases; thus the experimental values we obtained for $\Delta\alpha$ at the highest temperatures we achieved should be very close to the absolute value of the inverse phonon MFP and provide unique experimental data to be compared to existing models for acoustic attenuation.

Contribution of fission processes to the MFP temperature dependence remains small compared to scattering processes such as LA + TA → LA and LA + TA → TA, where LA (TA) denotes longitudinal (transverse) acoustic phonons. The latter process is forbidden when elastic isotropy is assumed but Herring [31] suggested that it should be very efficient in anisotropic systems. For such crystals, Herring showed that a longitudinal phonon, with energy $\hbar\omega_{ac}$ can interact with much higher-frequency slow and fast transverse thermal phonons (STA and FTA respectively) close to a symmetry axis along which there is degeneracy. A general expression for the sound absorption coefficient related to this process can be written as

$$\alpha_H(\omega_{ac}) = \frac{\hbar}{128\pi^2\rho^3 v_l}\int_{BZ}\frac{|\Lambda_{\mathbf{q},\mathbf{q}',\mathbf{q}+\mathbf{q}'}|^2[n(\omega')-n(\omega'+\omega_{ac})]}{\omega_{ac}\omega'(\omega_{ac}+\omega')} \times \delta[\omega_{ac}+\omega(\mathbf{q}',st)-\omega(\mathbf{q}+\mathbf{q}',ft)]d\mathbf{q}', \quad (2)$$

where $\Lambda_{\mathbf{q},\mathbf{q}',\mathbf{q}+\mathbf{q}'}$ is a coupling parameter, ρ the specific mass, v_l the longitudinal sound velocity along [100], $\mathbf{q}'$ the STA wave vector and $\hbar\omega' = \hbar\omega(\mathbf{q}',st)$ its energy; the indices st and ft mean slow and fast transverse, respectively, and $n(\omega')$ is the phonon population. Neglecting phonon dispersion, and using an elastic continuum approximation for the coupling parameter, Herring predicted an asymptotic behavior $B\nu^p T^{5-p}$ for α_H in the limit of low frequencies and low temperatures, where the exponent p depends on the crystal symmetry. Later on, Simons [38] derived an expression for the Herring processes contribution to sound attenuation in cubic crystals: in that case $p = 2$ and the prefactor B can be expressed in terms of second- and third-order elastic constants. The calculation for a longitudinal wave propagating along [100] gives

$$\alpha_{\mathrm{Hasy.}} = \frac{3\zeta(3)}{8\pi^2 v_l v_t^3}\frac{k_B^3}{\hbar^2}\frac{[E(h)-(1-h^2)K(h)]}{h^2(A^2-1)} \times \frac{(C_{155}+2C_{44}-C_{144})^2}{C_{11}C_{44}(C_{11}-C_{44})}\omega^2 T^3, \quad (3)$$

where $A = \frac{C_{44}+C_{12}}{C_{11}-C_{44}}$, $\zeta(3)$ is the Rieman ζ function of argument 3, $h = \frac{\sqrt{2A+1}}{A+1}$, $K(h)$ and $E(h)$ are the complete elliptic integral of the first and second kind [39]. Using the values $C_{11} = 121.07$, $C_{12} = 54.77$, $C_{44} = 60.36$ GPa [40], and $C_{155} = -269$, $C_{144} = 2$ GPa [41] for the GaAs second- and third-order elastic constants respectively, the contribution is

$$\alpha_{\mathrm{Hasy.}}(\mu\mathrm{m}^{-1}) = 3.96 \times 10^{-8}\nu^2 T^3, \quad (4)$$

where the acoustic frequency ν is expressed in THz. Herring himself [31] pointed out that this asymptotic behavior could be very limited. This appears clearly through the fact that Eq. (3) diverges when the crystal is isotropic ($A = 1$) while we expect a zero contribution from Herring processes in that case. We show in the Supplemental Material [42] how to solve this paradox and how limitation of the asymptotic limit depends strongly on the anisotropy factor A. Using expression 4 of $\alpha_{\mathrm{Hasy.}}$ in Fig. 3, it can be seen that $\alpha_{\mathrm{Hasy.}}$ prediction strongly underestimates the attenuation at 50 K up to 1 THz. This is not surprising since the asymptotic expression α_{Hasy} holds for a very limited frequency and temperature range as we shall see now. The exact calculation of α_H could be achieved using a microscopic model or *ab initio* calculations for the phonon dispersion and coupling parameters. However, calculation of

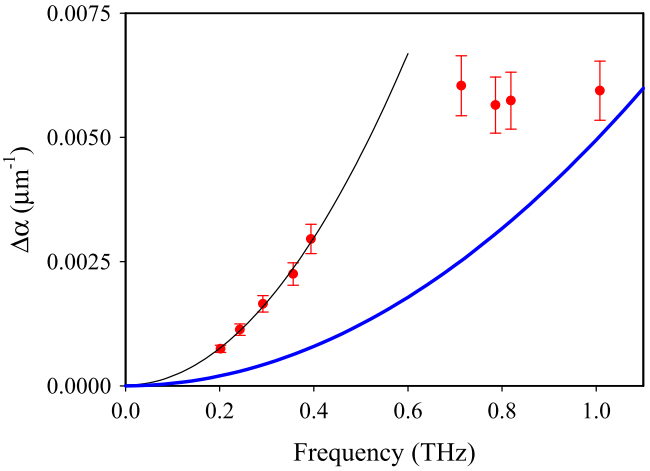

FIG. 3. Experimental frequency dependence of $\Delta\alpha(T)$ at 50 K (red circles). The thin black line is a frequency square fit, which works well up to 0.4 THz. Experimental data departs strongly from the estimation of Herring processes contribution with the asymptotic formula of Simons [38] (solid blue line).

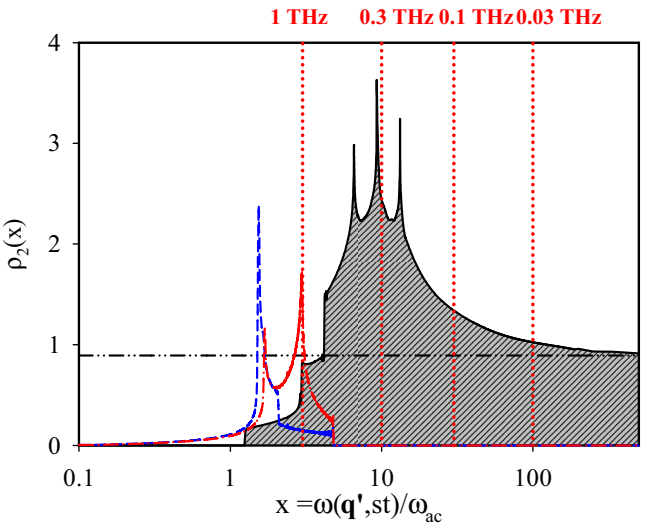

FIG. 4. Density $\rho_2(x)$ of rescaled phonons energies $x = \omega(\mathbf{q}',st)/\omega_{ac}$ satisfying the scattering selection rules for Herring processes LA + STA → FTA (solid black line), neglecting phonon modes dispersion. The black dashed-dotted line gives the asymptotic value of $\rho_2(x)$. The vertical dotted lines display the integration limits to obtain the two phonon density of states for different acoustic frequencies ν_{ac} assuming a cutoff frequency of 3 THz for the transverse phonons; densities $\rho_2(x)$ for LA + STA → LA (dashed blue line) and LA + FTA → LA (dash-dotted red line) processes are weaker but less affected by the cutoff frequency.

Herring processes occurrence for subterahertz longitudinal phonons would require a very fine mesh of the Brillouin zone. This work is beyond the scope of this paper but we will show that interesting information about the frequency behavior of α_H can be learned by considering the behavior of the two phonon density of states for Herring processes defined by

$$\rho_H(\omega_{ac}) = \int_{BZ} \delta[\omega_{ac} + \omega(\mathbf{q}',st) - \omega(\mathbf{q}+\mathbf{q}',ft)]d\mathbf{q}'. \quad (5)$$

Let us define the spherical coordinates (q',θ,φ) of the wave vector $\mathbf{q}'$. If we still neglect phonon dispersion, the energies $\hbar\omega(\mathbf{q}',st)$ and $\hbar\omega(\mathbf{q}+\mathbf{q}',ft)$ can be rescaled by the acoustic energy $\hbar\omega_{ac}$. The calculation of $\rho_H(\omega_{ac})$ requires then the determination of the values $x = \omega(\mathbf{q}',st)/\omega_{ac}$, which satisfy energy conservation $x(\theta,\varphi) = \omega(\mathbf{q}+\mathbf{q}',ft)/\omega_{ac} - 1$. The calculated density of these solutions $\rho_2(x)$ is given by

$$\rho_2(x) = \frac{x^2}{2\pi^2}\int_0^{2\pi} d\varphi \int_0^{\pi} d\theta \sin\theta\,\delta[x - x(\theta,\varphi)]. \quad (6)$$

This density is displayed in Fig. 4 neglecting phonon dispersion. We show, in the Supplemental Material [42], that the asymptotic value of $\rho_2(x)$ restricted to $\mathbf{q}'$ wave vectors close to the A_4 axes of a cubic system is given by

$$\lim_{x\to\infty} \rho_2(x) = \rho_{2,A_4}(x) = \frac{12}{\pi^2}\frac{\delta_{A_4}^2}{(1-\delta_{A_4}^2)(A^2-1)} K\left(\frac{\sqrt{2A+1}}{A+1}\right). \quad (7)$$

where $\delta_{A_4}^2 = \frac{C_{44}}{C_{11}}$. For GaAs it gives $\rho_{2,A_4}(x) = 0.894$. We can see in Fig. 4 that the exact calculation departs rapidly from this asymptotic value as x decreases. For example, another important contribution appears at smaller x values due to transverse phonons close to A_3 axes; in that case, the constant-frequency surfaces in wave vector space do not touch, as for A_4 axes, but just intersect. We show in the Supplemental Material [42] that the contribution $\rho_{2,A_3}(x)$ of these phonons is given by

$$\rho_{2,A_3}(x) = \frac{2}{\pi\chi_{A_3}^2}\sum_{\pm}(1\pm\delta)\sqrt{(1\pm\delta)^2 - \delta^2\chi_{A_3}^2}\,x^{-1}, \quad (8)$$

where $\delta = \frac{1}{3}\sqrt{\frac{C_{11}+C_{44}-C_{12}}{C_{11}}}$, $\chi_{A_3} = \frac{(A-1)(C_{11}-C_{44})}{9\delta^2 C_{11}}$ and signs (+) et (−) are given by the sign of the cosine of the angle between A_3 semi-axes and the [100] axis along which the acoustic wave under investigation is propagating. For GaAs it gives $\rho_{2,A_3}(x) = 7.62x^{-1}$, which is greater than $\rho_{2,A_4}(x)$ for $x < 10$. For $x = 20$, the exact calculation gives $[\rho_2(x) - \rho_{2,A_4}(x)]/\rho_{2,A_4}(x) = 80\%$. The previous analysis will first help us to define the frequency and temperature domain where the asymptotic expression α_{Hasy} is valid. If $\omega' \gg \omega_{ac}$, then the phonon population factor in Eq. (2) writes

$$n(\omega') - n(\omega'+\omega_{ac}) = \beta\hbar\omega_{ac}\frac{\exp(\beta\hbar\omega')}{(\exp(\beta\hbar\omega')-1)^2} \quad (9)$$

with $\beta = 1/k_BT$. Integration in Eq. (2) can be done using the dimensionless quantity $z = \beta h\nu_{ac}x$. The temperature behavior in the asymptotic limit is obtained assuming that we can integrate z from zero up to infinity. If we want to keep a lower bound for the integration quite small while satisfying the condition $x > 20$, we should fulfill a first condition, namely the value of frequency ν_{ac} (expressed in GHz) should be lower than the value of temperature T (expressed in K): $\nu_{ac}(\text{GHz}) < T(\text{K})$. Moreover, the dispersion on transverse phonon branches cannot be neglected in GaAs for frequencies above 1 THz [43]. Thus, temperature should be small enough to keep phonon populations above 1 THz negligible. This leads

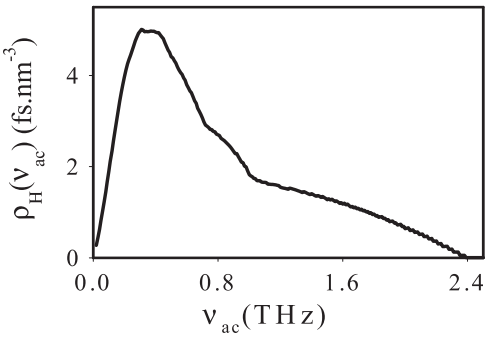

FIG. 5. Integrated two phonon density of states $\rho_H(\nu_{ac})$ for Herring processes. The maximum is reached at 0.4 THz and Herring processes clearly break down in the range 0.5–1 THz.

to the second condition: $T < 10$ K for an error of 20% in the integration. These two conditions show that the temperature and frequency domains where $\alpha(\nu_{ac}) = 3.96 \times 10^{-8} \nu_{ac}^2 T^3$ holds are drastically limited.

We will now consider how Herring processes behave beyond these frequency and temperature ranges. A key point to answer this question is the fact that transverse phonons frequencies in GaAs have a cutoff at approximately 3 THz [43]. In order to obtain the two phonon density of states defined by:

$$\rho_H(\omega_{ac}) \simeq \frac{\omega_{ac}^2}{4\pi \langle v_t \rangle^3} \int_0^{x_{\max}} \rho_2(x) dx, \qquad (10)$$

where $\langle v_t \rangle$ is a transverse velocity averaged on the whole Brillouin zone, the integration has to be limited to a maximum value $x_{\max}=3/\nu_{ac}$ (ν_{ac} in THz), indicated by vertical dotted lines in Fig. 4 for different acoustic frequencies. The resulting integrated density of states $\rho_H(\omega_{ac})$ is displayed in Fig. 5. First, it increases rapidly, and then reaches a maximum for a few hundreds of GHz and at the end drops above 1 THz. The contribution of Herring processes to the attenuation of subterahertz longitudinal acoustic waves should be above the asymptotic prediction given by Simons's formula, before reaching a maximum. These Herring processes then break down above 1 THz. Meanwhile the other scattering processes LA + STA → LA and LA + FTA → LA, whose contributions to $\rho_2(x)$ are displayed on Fig. 4 should have a negligible contribution at frequencies below 0.1 THz. They continuously increase with frequency and could partially compensate for the Herring processes breakdown above 1 THz. More likely, the plateau we observed experimentally is the signature of this breakdown, which is largely due to the characteristic shapes of transverse phonons curves in GaAs, which become very flat after the half of the Brillouin zone and have a low cutoff frequency; this fact is general for crystals with long-range interactions such as covalent semiconductors. Thus, the same statement about Herring processes breakdown should also hold for crystals with equivalent structure and bonding such as silicon and germanium: our calculations indicate that indeed two phonons density of states exhibits a maximum at 0.7 THz in silicon and germanium. This fact has also been shown with calculations performed for a fcc lattice with nearest-neighbor central forces [44], which clearly demonstrates saturation of Herring processes contributions at temperatures much lower than the Debye temperature for a frequency range in good agreement with our observations in GaAs.

IV. CONCLUSION

We have measured the anharmonic contribution to the MFP of subterahertz coherent acoustic phonons in GaAs at temperatures much below the Debye temperature. Our experimental results show an unexpected plateau for the acoustic absorption above 0.7 THz up to 1 THz. We gave qualitative arguments to demonstrate that Herring processes give the dominant contribution to this absorption up to 0.3–0.4 THz but become rapidly inefficient, due to the low-frequency cutoff of transverse phonons in GaAs, giving rise to the observed plateau. This effect is responsible for the long MFP [$l = (2\alpha)^{-1} = 50\,\mu$m] we measured at 1 THz at 60 K. An extrapolation with a T^{-1} dependence at room temperature leads to a MFP of 10 μm, which is surprisingly large but could explain the recent indirect observations of long MFP in crystalline semiconductors, which have been inferred from measurements with the thermal conductivity spectroscopy technique [5]; this value is also close to the extrapolation to low-frequency modes of first-principles calculations of the phonons relaxation times for normal and umklapp scattering processes in GaAs [12] and to a rough estimation deduced from lifetime measurement of an acoustic nanocavity [45]. Thus, while the Herring processes' contribution to longitudinal phonon absorption is dominant up to a few hundreds of GHz, their breakdown, which is a general statement, provides a frequency window where subterahertz coherent acoustic waves can propagate over macroscopic distances, even at room temperatures. These results are particularly appealing for phonon imaging using nanometric acoustic waves.

[1] Y. K. Koh and D. G. Cahill, Phys. Rev. B **76**, 075207 (2007).
[2] A. J. Minnich, Phys. Rev. Lett. **109**, 205901 (2012).
[3] A. J. Minnich, J. A. Johnson, A. J. Schmidt, K. Esfarjani, M. S. Dresselhaus, K. A. Nelson, and G. Chen, Phys. Rev. Lett. **107**, 095901 (2011).
[4] K. T. Regner, D. P. Sellan, Z. Su, C. H. Amon, A. J. H. McGaughey, and J. Malen, Nature Commun. **4**, 1640 (2013).
[5] J. P. Freedman, J. H. Leach, E. A. Preble, Z. Sitar, R. F. Davis, and J. A. Malen, Sci. Rep. **3**, 2963 (2013).
[6] L. Zeng, K. C. Collins, Y. Hu, M. N. Luckyanova, A. A. Maznev, S. Huberman, V. Chiloyan, J. Zhou, X. Huang, K. A. Nelson, and G. Chen, Sci. Rep. **5**, 17131 (2015).
[7] J. A. Johnson, A. A. Maznev, J. Cuffe, J. K. Eliason, A. J. Minnich, T. Kehoe, Clivia M. Sotomayor Torres, G. Chen, and K. A. Nelson, Phys. Rev. Lett. **110**, 025901 (2013).
[8] T.-K. Hsiao, H.-K. Chang, S.-C. Liou, M.-W. Chu, S.-C. Lee, and C.-W. Chang, Nature Nanotech. **8**, 534 (2013).
[9] J. Cuffe, J. K. Eliason, A. A. Maznev, K. C. Collins, J. A. Johnson, A. Shchepetov, M. Prunnila, J. Ahopelto, C. M.

Sotomayor Torres, G. Chen, and K. A. Nelson, Phys. Rev. B **91**, 245423 (2015).
[10] A. Ward, D. A. Broido, D. A. Stewart, and G. Deinzer, Phys. Rev. B **80**, 125203 (2009).
[11] A. Ward and D. A. Broido, Phys. Rev. B **81**, 085205 (2010).
[12] T. Luo, J. Garg, J. Shiomi, K. Esfarjani, and G. Chen, Europhys. Lett. **101**, 16001 (2013).
[13] W. Chen, H. J. Maris, Z. Wasilewski, and S.-I. Tamura, Philos. Mag. B **70**, 687 (1994).
[14] H.-Y. Hao and H. J. Maris, Phys. Rev. B **63**, 224301 (2001).
[15] J.-Y. Duquesne and B. Perrin, Phys. Rev. B **68**, 134205 (2003).
[16] B. C. Daly, K. Kang, Y. Wang, and D. G. Cahill, Phys. Rev. B **80**, 174112 (2009).
[17] T. C. Zhu, H. J. Maris, and J. Tauc, Phys. Rev. B **44**, 4281 (1991).
[18] P. Emery and A. Devos, Appl. Phys. Lett. **89**, 191904 (2006).
[19] A. Yamamoto, T. Mishina, Y. Masumoto, and M. Nakayama, Phys. Rev. Lett. **73**, 740 (1994).
[20] A. Bartels, T. Dekorsy, H. Kurz, and K. Köhler, Phys. Rev. Lett. **82**, 1044 (1999).
[21] P. Hawker, A. J. Kent, L. J. Challis, A. Bartels, T. Dekorsy, H. Kurz, and K. Köhler, Appl. Phys. Lett. **77**, 3209 (2000).
[22] A. Huynh, B. Perrin, N. D. Lanzillotti-Kimura, B. Jusserand, A. Fainstein, and A. Lemaître, Phys. Rev. B **78**, 233302 (2008).
[23] L. Belliard, A. Huynh, B. Perrin, A. Michel, G. Abadias, and C. Jaouen, Phys. Rev. B **80**, 155424 (2009).
[24] A. Huynh, B. Perrin, B. Jusserand, and A. Lemaître, Appl. Phys. Lett. **99**, 191908 (2011).
[25] M. F. Pascual-Winter, A. Fainstein, B. Jusserand, B. Perrin, and A. Lemaître, Phys. Rev. B **85**, 235443 (2012).
[26] A. Huynh, B. Perrin, and A. Lemaître, Ultrasonics **56**, 66 (2015).
[27] A. J. Kent, N. M. Stanton, L. J. Challis, and M. Henini, Appl. Phys. Lett. **81**, 3497 (2002).
[28] T.-M. Liu, S.-Z. Sun, C.-F. Chang, C.-C. Pan, G.-T. Chen, J.-I. Chyi, V. Gusev, and C.-K. Sun, Appl. Phys. Lett. **90**, 041902 (2007).
[29] A. A. Maznev, F. Hofmann, A. Jandl, K. Esfarjani, M. T. Bulsara, E. A. Fitzgerald, G. Chen, and K. A. Nelson, Appl. Phys. Lett. **102**, 041901 (2013).
[30] B. Jusserand, A. N. Poddubny, A. V. Poshakinskiy, A. Fainstein, and A. Lemaître, Phys. Rev. Lett. **115**, 267402 (2015).
[31] C. Herring, Phys. Rev. **95**, 954 (1954).
[32] N. D. Lanzillotti-Kimura, A. Fainstein, B. Perrin, B. Jusserand, L. Largeau, O. Mauguin, and A. Lemaître, Phys. Rev. B **83**, 201103 (2011).
[33] N. D. Lanzillotti-Kimura, A. Fainstein, A. Lemaître, B. Jusserand, and B. Perrin, Phys. Rev. B **84**, 115453 (2011).
[34] R. Legrand, A. Huynh, B. Perrin, N. D. Lanzillotti-Kimura, and A. Lemaître, Int. J. Thermophys. **34**, 1727 (2013).
[35] H. J. Maris, in *Physical Acoustics*, Vol. 8, edited by W. P. Mason and R. N. Thurston (Academic Press, New York, 1971), p. 279.
[36] A. Berke, A. P. Mayer, and R. K. Wehner, J. Phys. C **21**, 2305 (1988).
[37] H. J. Maris and S. Tamura, Phys. Rev. B **84**, 024301 (2011).
[38] S. Simons and J. M. Ziman, Mathematical Proceedings of the Cambridge Philosophical Society **53**, 702 (1957).
[39] G. A. Korn and T. M. Korn, *Mathematical Handbook for Scientists and Engineers* (McGraw-Hill, New York, 1961), p. 709.
[40] R. I. Cottam and G. A. Saunders, J. Phys. C **6**, 2105 (1973).
[41] H. McSkimin and P. Andreatch Jr., J. Appl. Phys. **38**, 2610 (1967).
[42] See Supplemental Material at http://link.aps.org/supplemental/10.1103/PhysRevB.93.184304 for (i) a description of the calculation of the two-phonon density of states, (ii) a derivation of the Herring processes' contribution to the two phonon density of states for phonon propagating along symmetry axes and (iii) derivation of an analytical expression of this same quantity in the limit of a weak anisotropy.
[43] J. L. T. Waugh and G. Dolling, Phys. Rev. **132**, 2410 (1963).
[44] S. Tamura and H. J. Maris, Phys. Rev. B **51**, 2857 (1995).
[45] G. Rozas, M. F. Pascual Winter, B. Jusserand, A. Fainstein, B. Perrin, E. Semenova, and A. Lemaître, Phys. Rev. Lett. **102**, 015502 (2009).